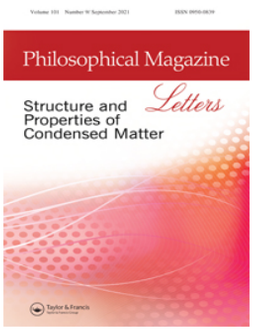

Philosophical Magazine Letters

ISSN: (Print) (Online) Journal homepage: https://www.tandfonline.com/loi/tphl20

The relation between grain boundary precipitate formation and adjacent grain orientations in Al-Mg-Si(-Cu) alloys

Calin D. Marioara, Tore Børvik & Odd-Sture Hopperstad

To cite this article: Calin D. Marioara, Tore Børvik & Odd-Sture Hopperstad (2021) The relation between grain boundary precipitate formation and adjacent grain orientations in Al-Mg-Si(-Cu) alloys, Philosophical Magazine Letters, 101:9, 370-379, DOI: 10.1080/09500839.2021.1946188

To link to this article: https://doi.org/10.1080/09500839.2021.1946188

Published online: 11 Jul 2021.

PHILOSOPHICAL MAGAZINE LETTERS
2021, VOL. 101, NO. 9, 370–379
https://doi.org/10.1080/09500839.2021.1946188

The relation between grain boundary precipitate formation and adjacent grain orientations in Al-Mg-Si(-Cu) alloys

Calin D. Marioara[a], Tore Børvik[b,c] and Odd-Sture Hopperstad[b,c]

[a]Materials and Nanotechnology, SINTEF Industry, Trondheim, Norway; [b]Structural Impact Laboratory (SIMLab), Department of Structural Engineering, NTNU – Norwegian University of Science and Technology, Trondheim, Norway; [c]Centre for Advanced Structural Analysis (CASA), NTNU, Trondheim, Norway

ABSTRACT

The occurrence of grain boundary precipitates was investigated with respect to the crystallographic orientation of the adjacent grains in extruded AA6110, AA6063 and AA6061 alloys brought to T6 temper. It was found that the requirement for grain boundary precipitate formation is for the adjacent grains to have <100>Al directions or {100}Al planes parallel to the grain boundary plane. The highest density of grain boundary precipitates was present when this requirement was fulfilled by both adjacent grains.

ARTICLE HISTORY
Received 14 January 2021
Accepted 15 June 2021

KEYWORDS
Transmission electron microscopy; grain boundary precipitates; crystallographic orientation

Introduction

Al-Mg-Si(-Cu) (6xxx) alloys are widely used as structural materials due to their medium strength, high ductility, good corrosion resistance and lightweight properties [1]. A common processing route consists of casting, homogenisation and extrusion as the main forming process and artificial ageing (AA) as the final step to achieve the desired combination of properties. The most important of these is often strength, which is generated by the nucleation and growth in the Al matrix of large numbers of metastable nano-sized precipitates. Depending on the AA temperature and holding time, precipitates form with different crystal structures, number densities and size distributions [2–4]. The driving force for precipitation is given by the formation of a supersaturated solid solution upon rapid cooling from extrusion, or solution heat treatment before AA. In this state, the solute elements are uniformly distributed in the Al matrix, together with a high density of quenched-in vacancies. Because Al alloys are polycrystalline, fast diffusion of vacancies to grain boundaries (GBs) take place during AA, which also transports solute. The consequence

CONTACT Calin D. Marioara calin.d.marioara@sintef.no

is the formation of precipitation free zones (PFZs) along GBs, and solute enrichment of GB planes.

Several works have shown that this solute will form GB precipitates during AA [5–7]. It is believed these microstructures play an important role in processes such as intergranular corrosion (IGC) [6,7], and on the ductility and toughness [8–11] of the alloy. Experimental observations have indicated large variations in the amount of GB precipitates between different GBs in the same material, and even along the same GB. In the latter, one segment could have no precipitation, and another a high density as the GB is changing orientation [7]. These observations indicate an effect related to GB orientations with the adjacent grains. Also, the GB precipitates are confirmed to consist of metastable types, with crystal structures similar to bulk precipitates [5–7].

In 6xxx alloys the bulk precipitates have needle/rod/lath morphologies, with the main growth direction along <100>Al, which coincides with their highest coherency with the Al matrix. It implies that if similar precipitates nucleate at GBs, they need at least one <100>Al type direction of one adjacent grain to be parallel to the GB plane. Image analysis of GB precipitates from previous studies show that at least one of the adjacent grains is close to a <001>Al orientation along the viewing direction [5–7]. However, no systematic study has been performed so far connecting the orientations of adjacent grains with the presence and density of GB precipitates. In this work we investigated various GBs for the presence of GB precipitates and recorded the approximate orientation of the adjacent grains, to determine if any connection can be established between the two parameters. For this purpose, we selected three industrial alloys based on their high relevance for applications in safety components in the automotive industry. Two alloys had recrystallised grain structure, while the third had non-recrystallised (fibrous) grain structure and thus a different crystallographic texture.

Materials and methods

Three aluminium alloys with compositions given in Table 1 were direct-chill (DC) cast and homogenised [12]. Alloys AA6063 and AA6110 were extruded into bars with 6 mm thickness and 40 mm width before water quenching. During the following 1–3 h from extrusion, the profiles were deformed to lengths corresponding to a strain of 0.5%. Further, the profiles were stored for 48 h at room temperature (RT) before AA to peak hardness was performed

Table 1. Alloy compositions (wt%).

Alloy/Element	Mg	Si	Cu	Fe	Mn	Zn	Ti	Cr
AA6061	0.903	0.621	0.204	0.209	0.038	0.054	0.106	0.060
AA6063	0.470	0.512	0.001	0.206	0.047	0.003	0.006	0.001
AA6110	0.828	0.720	0.203	0.196	0.506	0.003	0.026	0.157

at 185°C using a heating rate of 175°C/h and holding time of 8 h. The profiles were then air-cooled to RT. After homogenisation, billets of alloy AA6061 were first soft annealed by rapid heating from a cold oven to 410°C where they were held for 4 h before air cooling to RT. The soft-annealed billets were then extruded, and solution heat treated using a heating rate of 400°C/h and 10 min holding time at 560°C before water quench. The profiles were then stretched, stored at RT and artificially aged as described above for the other two alloys.

Optical Microscopy (OM) and Scanning Electron Microscopy (SEM) showed that alloys AA6063 and AA6061 have recrystallised grain structures, while alloy AA6110 has a fibrous, non-recrystallised structure. Electron Backscatter Diffraction (EBSD) measurements indicated a strong cube texture with a marked Goss component for alloys AA6061 and AA6063, while the AA6110 alloy had a cube texture with orientations along the β-fibre, which go from the Copper and Brass orientation and through the S component. These are typical for recrystallised (AA6063 and AA6061) and non-recrystallised (AA6110) alloys. Detailed information about the grain size and texture of these alloys can be found in [13]. Similar textures have been reported for other extruded 6xxx series alloys [14,15].

Transmission Electron Microscopy (TEM) was performed along the extrusion direction, and specimens were prepared by electropolishing from the middle of 6 mm thick extrusion plates. For imaging, a field emission gun (FEG) Jeol 2100F TEM operated at 200 kV was used in bright field, diffraction and Annular Dark Field Scanning TEM (ADF-STEM) modes. X-ray energy dispersive spectroscopy (EDS) mapping was performed with an Oxford Instruments silicon drift detector and INCA software in analytical STEM mode using 1.5 nm probe size and approximately 3 nm step size.

The approximate orientation of the Al matrix along the viewing direction was estimated by comparison of kinematical simulated diffraction patterns using the software CrystalKit (https://www.totalresolution.com/) with the experimentally recorded selected area diffraction patterns (SADPs) from grains adjacent to an edge-on oriented GB plane.

Results and discussion

A typical grain structure in the fibrous AA6110 alloy is presented in Figure 1. It is characterised by two distinct areas with different crystallographic orientations separated by a High Angle GB (HAGB). The upper part has an orientation close to <001>Al, while the lower part is oriented close to <112>Al. Each area contained sub-grains separated by Low Angle GBs (LAGBs). According to the SADPs in Figure 1, the upper sub-grains have slight rotations around a common <001>Al direction, while the relative orientation of the <112>Al oriented lower sub-grains was difficult to estimate. To investigate the presence

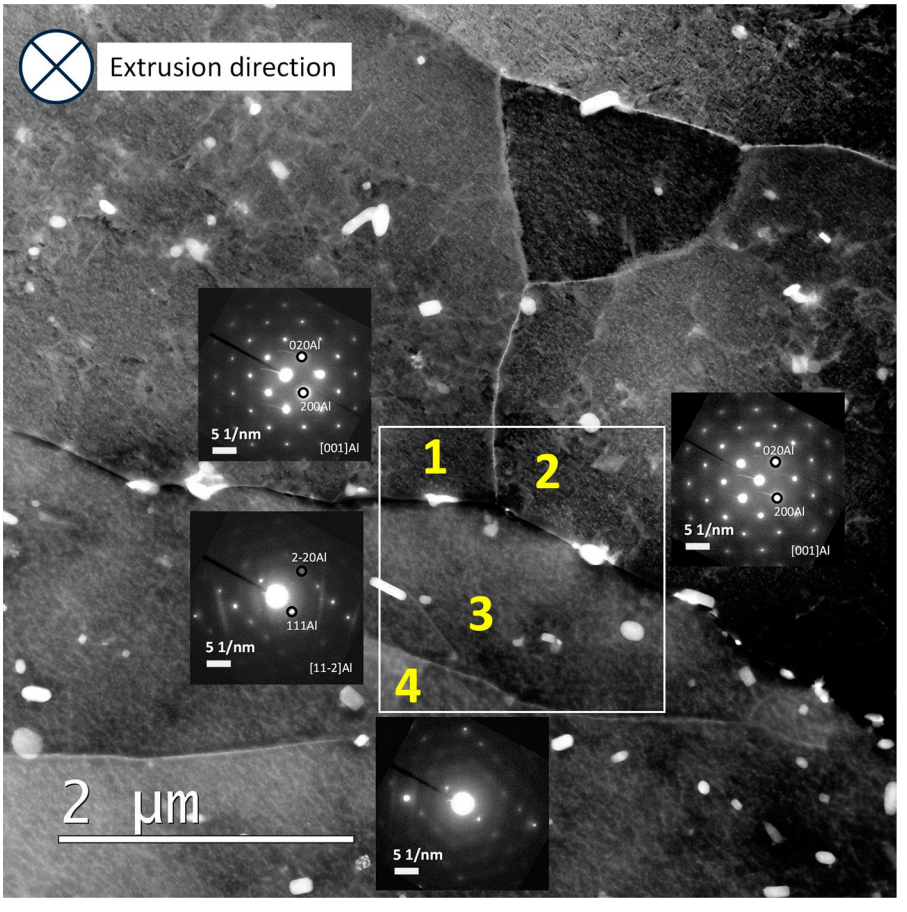

Figure 1. Typical grain microstructure in the fibrous alloy 6110. The orientation of the different grains is indicated by the SADPs. Four grains/sub-grains of interest are numbered in the square area delimited by white lines, which was selected for EDS mapping.

of GB precipitates on the various types of GBs, EDS maps were performed on different parts of the volume represented in Figure 1, and the results are shown in Figure 2. In these maps, the presence of metastable precipitates is indicated by their Si, Mg and Cu compositions (at the same locations), while the dispersoids are identified by their composition containing Si, Mn and Fe (not shown). All these phases also contain Al, which is not shown. Based on the findings in [16], the presence of only Cu or Mg or both as continuous weak signals along a GB was interpreted as elemental segregation, while the presence of strong signals of Mg, Si and Cu, as the presence of metastable precipitates.

The following observations can be made:

- The HAGB delimiting the <001>Al and <112>Al oriented areas does not contain GB precipitates but shows segregation of Mg and Cu. The GB is pinned by dispersoids, on which large Mg-Si-Cu precipitates have nucleated.

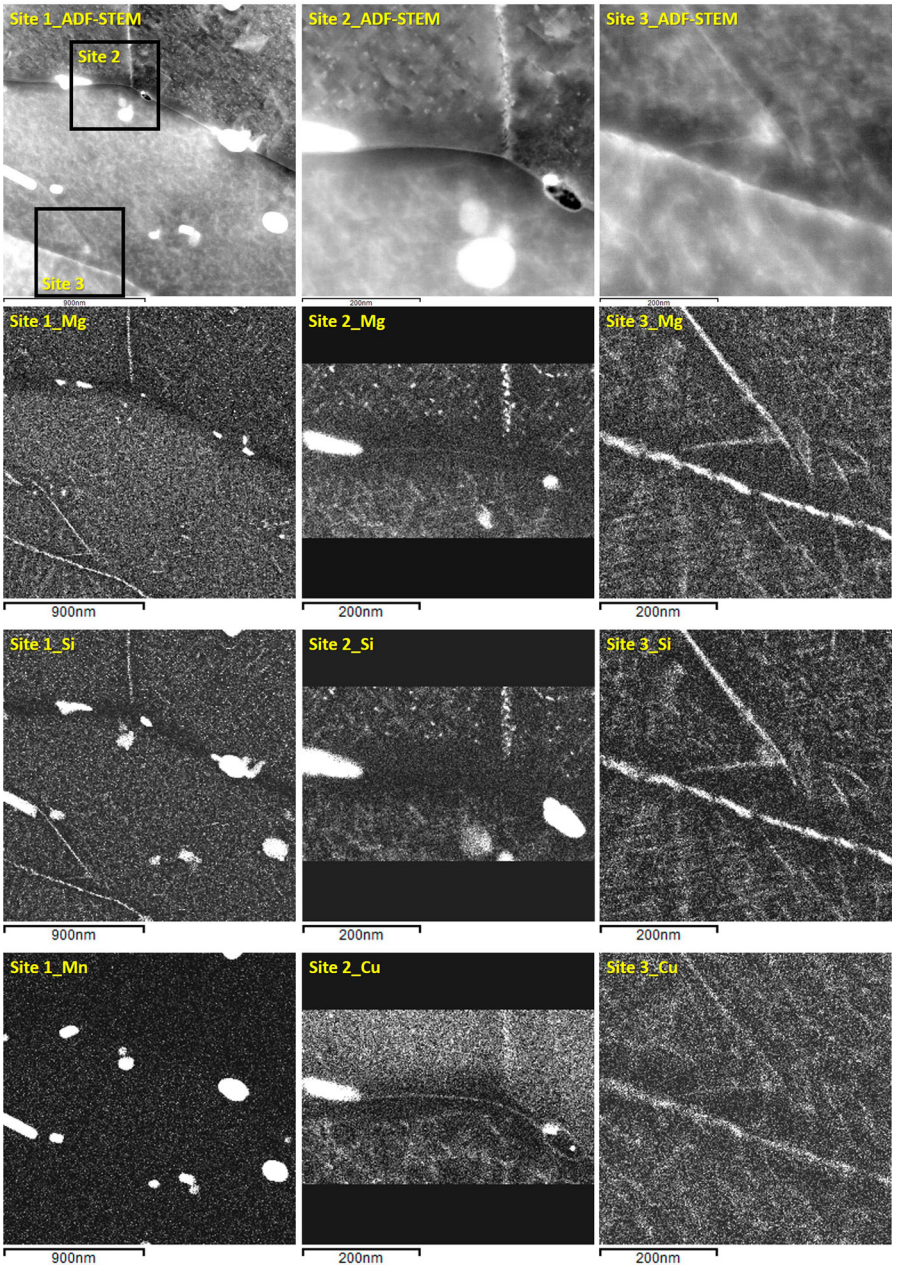

Figure 2. ADF-STEM images and corresponding elemental EDS maps of areas imaged in Figure 1. The Si map of Site 3 is used in Figure 3.

- All sub-grain boundaries contain a high density of GB precipitates. In the case of the LAGB between sub-grains 1 and 2, which share a common <001>Al direction, dense dot-like precipitates are observed in the Mg and Si maps (see Site 2 in Figure 2). A higher magnification bright field image in Figure 3a indicates these are needle precipitates viewed in cross-section.

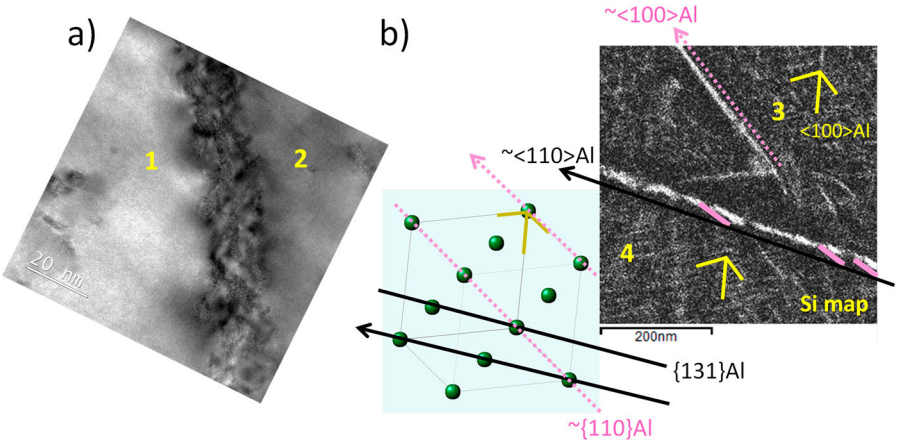

Figure 3. (a) Bright field TEM image of the LAGB between sub-grains 1 and 2 which indicates high density of needles oriented along <001>Al and viewed in cross-section. (b) Needle precipitates between sub-grains 3 and 4 are included in a {110}Al plane (upper part) and are nucleated on a {131}Al plane (lower part). In both parts the needles grow along the same <100>Al direction and are viewed at an angle to their lengths. In the figure the directions are marked with arrows and edge-on planes with lines. The pink short and thicker lines in the lower part are used to indicate that the needle precipitates nucleate along <100>Al and are at an angle with the {131}Al plane viewed edge-on.

This sub-grain boundary and the nucleated precipitates are very similar to the case in Fig. 5 of [16]. There atomically resolved HAADF-STEM imaging reveals that most precipitates are Cu-containing disordered metastable precipitates.

- In the case of the LAGBs between sub-grains 3 and 4, Figure 3b shows that in the upper part the needle-shaped GB precipitates extend along one <100>Al direction and are contained in a {110}Al plane viewed edge-on (see the pink dotted arrow and line, respectively). For the lower part, the needle GB precipitates extend along the same <100>Al direction as in the upper part (see the pink short, full lines), but they nucleate on a {131}Al plane viewed edge-on (see the black line and arrow). Therefore, in this part the precipitates are not included in the GB plane and the GB acts as a dislocation line.

In addition to the above-mentioned case, two more GB configurations are found to yield a high density of GB precipitates. In one case both adjacent grains have {100}Al planes parallel to the GB plane, while in the other case one adjacent grain has a <001>Al direction and the other adjacent grain a {100}Al plane parallel to the GB plane. Examples are given in Figure 4, from alloys AA6061 and AA6063. For each alloy, one GB with edge-on orientation is imaged in ADF-STEM mode, together with the adjacent PFZs and bulk of the grains. The next two images in the row show corresponding Mg and Si maps that indicate high densities of GB precipitates. Due to the elongated appearance of the locations of the Mg and Si signals, the GB precipitates

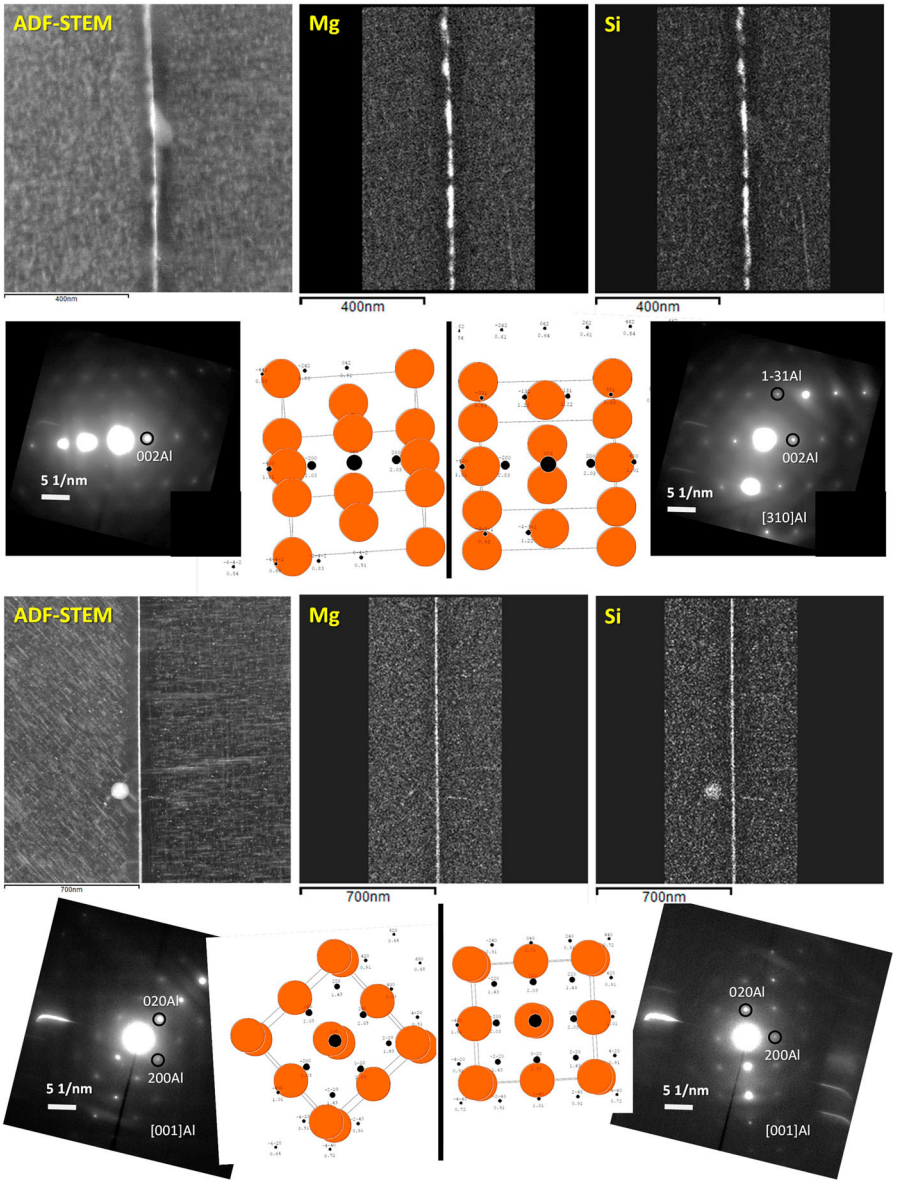

Figure 4. ADF-STEM images, corresponding EDS maps, SADPs and relative crystallographic orientation of the adjacent grains in respect to the GB plane viewed edge-on. The upper two rows of images show an example from alloy AA6061, while the lower two rows show an example from alloy AA6063.

must be needle-shaped viewed at an angle to their lengths. This is verified in the next row of images, that show SADPs from each adjacent grain and reconstructed kinematical diffraction patterns overlapped with the corresponding orientation of the Al matrix (for one Al unit cell). In the example from the AA6061 alloy, two {100}Al planes are nearly parallel to the GB plane, and all the <100>Al directions included in them are viewed at an angle. In the

example from the AA6063 alloy, the left-hand side grain has one <001>Al direction parallel to the GB plane (and viewed along), while the right-hand side grain has one <100>Al direction (viewed perpendicular) and one <001>Al direction (viewed along) (and these two directions are included in an {100}Al plane) parallel to the GB plane. In this case, we can also say that the two adjacent grains are rotation grains around a common <001>Al direction.

All examples of GBs with dense nucleation of GB precipitates found in this work exhibited one <100>Al direction or one {100}Al plane of one or both adjacent grains being parallel to the GB plane. It should be mentioned that the TEM analysis was performed on foils with thicknesses of around 100 nm, to ensure electron transparency. In such thin specimens, the grains are apparently connected by GB planes. In reality, as bulk Al is a three-dimensional entity, grains are connected by surfaces that constantly change orientation. Therefore, the same two grains can generate GB precipitates on one surface of the GB, and be precipitate-free on other surfaces, depending on the specific local orientation of the GB in respect to the crystallographic orientation of the grains. One such example is shown in [7]. In this context, for a given thermomechanical treatment, the concept of texture and the notion of HAGB or LAGB should be described more accurately by introducing a parameter that measures the fraction of GB area aligning with <100>Al directions or {100}Al planes of the adjacent grains for an estimation of the amount of GB precipitates present in a given condition. If precipitate-containing GBs have different behaviour under stress than the precipitate-free GBs, estimation of GB fraction with precipitates will improve our understanding of material deformation and fracture.

Conclusions

This study concludes that high-density precipitation on GBs must consist of metastable phases. In the case of 6xxx alloys, these phases have lath/rod/needle morphologies with main coherency directions along the crystallographic <100>Al. Therefore, at GBs this criterion is fulfilled only when at least one <100>Al direction or a {100}Al plane of one of the adjacent grains is parallel to the GB plane. The highest density of GB precipitates was observed when both grains had {100}Al planes parallel to the GB plane, and when one grain had the plane and the other a <100>Al direction parallel to the GB plane. Another situation generating a high density of GB precipitates is when the adjacent grains have a common <100>Al direction in the GB plane. GBs with random orientations did not contain dense precipitation of Mg-Si phases.

Acknowledgements

The authors gratefully appreciate the financial support from NTNU and the Research Council of Norway through the FRINATEK Programme, Project No. 250553 (FractAl).

Disclosure statement

No potential conflict of interest was reported by the author(s).

Funding

The financial support was provided from NTNU and the Research Council of Norway through the FRINATEK Programme, Project No. 250553 (FractAl).

Notes on contributors

Calin D. Marioara is a senior research scientist, with SINTEF Industry since 2001. He earned his doctoral degree at the Norwegian University of Science and Technology (NTNU) in 2001.

Tore Børvik is professors at the Department of Structural Engineering, NTNU. He earned his doctoral degree in 2001 within applied mechanics. He is a senior advisor for the Norwegian Defence Estates Agency. He was the head of the research programme Optimal Energy Absorption and Protection at CRI-SIMLab at NTNU from 2007 – 2014, and he is the co-director and head of the research programme Protective Structures in CRI-CASA at NTNU from 2015 – 2023.

Odd-Sture Hopperstad is professors at the Department of Structural Engineering, NTNU. He earned his doctoral degree at the Norwegian Institute of Technology (NTH) in 1993 and for this work he received the ESSO prize for best doctoral degree in fundamental research. He was appointed professor at NTNU in 1998. He is a member of the Norwegian Academy of Technological Sciences and the Royal Norwegian Society of Sciences and Letters. Currently he is Research Director of the Centre of Research-based Innovation CASA and principal investigator of the Toppforsk project FractAl at NTNU.

References

[1] K. Qvale, O.S. Hopperstad, O. Reiso, U.H. Tundal, C.D. Marioara, and T. Børvik, *An experimental study on pre-stretched double-chamber 6000-series aluminium profiles subjected to quasi-static and dynamic axial crushing*. Thin-Walled Struct. 158 (2021), Article Number: 107160, DOI:10.1016/j.tws.2020.107160.

[2] T. Saito, E.A. Mortsell, S. Wenner, C.D. Marioara, S.J. Andersen, J. Friis, K. Matsuda, and R. Holmestad, *Atomic structures of precipitates in Al-Mg-Si alloys with small additions of other elements*. Adv. Eng. Mater. 20(7) (2018), Article Number: 1800125, DOI:10.1002/adem.201800125.

[3] J.K. Sunde, C.D. Marioara, and R. Holmestad, *The effect of low Cu additions on precipitate crystal structures in overaged Al-Mg-Si(-Cu) alloys*. Mater. Charact. 160 (2020), Article Number: 110087, DOI: 10.1016/j.matchar.2019.110087.

[4] C.D. Marioara, S.J. Andersen, T.N. Stene, H. Hasting, J. Walmsley, A.T.J. Van Helvoort, and R. Holmestad, *The effect of Cu on precipitation in Al-Mg-Si alloys*. Philos. Mag. 87(23) (2007), pp. 3385–3413. DOI: 10.1080/14786430701287377.

[5] W.C. Yang, S.X. Ji, Z. Li, and M.P. Wang, *Grain boundary precipitation induced by grain crystallographic misorientations in an extruded Al-Mg-Si-Cu alloy*. J. Alloys Compd. 624 (2015), pp. 27–30. DOI: 10.1016/j.jallcom.2014.10.206.

[6] S.K. Kairy, T. Alam, P.A. Rometsch, C.H.J. Davies, R. Banerjee, and N. Birbilis, *Understanding the origins of intergranular corrosion in copper-containing Al-Mg-Si alloys*. Metall. Mater. Trans. A 47A(3) (2016), pp. 985–989. DOI:10.1007/s11661-015-3296-3.

[7] A. Lervik, T. Danbolt, T. Furu, R. Holmestad, and O. Lunder, *Comparing intergranular corrosion in Al-Mg-Si-Cu alloys with and without alpha-Al(Fe,Mn,Cu)Si particles*. Mater. Corros. – Werkst. Korros. 72, pp. 575-584 (2021). DOI: 10.1002/maco.202011954.

[8] A.K. Vasudévan, and R.D. Doherty, *Grain boundary ductile fracture in precipitation hardened aluminum alloys*. Acta Metall. 35(6) (1987), pp. 1193–1219. DOI: 10.1016/0001-6160(87)90001-0.

[9] T.F. Morgeneyer, M.J. Starink, S.C. Wang, and I. Sinclair, *Quench sensitivity of toughness in an Al alloy: direct observation and analysis of failure initiation at the precipitate-free zone*. Acta Mater. 56(12) (2008), pp. 2872–2884. DOI: 10.1016/j.actamat.2008.02.021.

[10] Y. Chen, K.O. Pedersen, A.H. Clausen, and O.S. Hopperstad, *An experimental study on the dynamic fracture of extruded AA6xxx and AA7xxx aluminium alloys*. Mater. Sci. Eng. A 523(1–2) (2009), pp. 253–262. DOI: 10.1016/j.msea.2009.06.007.

[11] B.H. Frodal, E. Christiansen, O.R. Myhr, and O.S. Hopperstad, *The role of quench rate on the plastic flow and fracture of three aluminium alloys with different grain structure and texture*. Int. J. Eng. Sci. 150 (2020), Article Number: 103257, DOI: 10.1016/j.ijengsci.2020.103257

[12] S. Thomesen, O.S. Hopperstad, O.R. Myhr, and T. Børvik, *Influence of stress state on plastic flow and ductile fracture of three 6000-series aluminium alloys*. Mater. Sci. Eng. A 783 (2020), Article Number: 139295, DOI: 10.1016/j.msea.2020.139295

[13] S. Thomesen, *Plastic Flow and Fracture of Isotropic and Anisotropic 6000-Series Aluminium Alloys: Experiments and Numerical Simulations*, Doctoral thesis, NTNU, 2019:312, ISBN 978-82-326-4220-5 (print), ISBN 978-82-326-4221-2 (electronic), ISSN 1503-8181

[14] B.H. Frodal, K.O. Pedersen, T. Børvik, and O.S. Hopperstad, *Influence of pre-compression on the ductility of AA6xxx aluminium alloys*. Int. J. Fract. 206(2) (2017), pp. 131–149. DOI: 10.1007/s10704-017-0204-4.

[15] M. Khadyko, S. Dumoulin, T. Børvik, and O.S. Hopperstad, *An experimental-numerical method to determine the work-hardening of anisotropic ductile materials at large strains*. Int. J. Mech. Sci. 88 (2014), pp. 25–36. DOI: 10.1016/j.ijmecsci.2014.07.001.

[16] A. Lervik, S. Wenner, O. Lunder, C.D. Marioara, and R. Holmestad, *Grain boundary structures and their correlation with intergranular corrosion in an extruded Al-Mg-Si-Cu alloy*. Mater. Charact. 170 (2020), Article Number: 110695, DOI: 10.1016/j.matchar.2020.110695